DRDC Ottawa SL 2003-012

Application of adaptive joint time–frequency algorithm for focusing distorted ISAR images from simulated and measured radar data

T. Thayaparan, G. Lampropoulos, S.K. Wong and E. Riseborough

Abstract: An adaptive joint time–frequency algorithm has been applied and evaluated for focusing distorted ISAR (inverse synthetic aperture radar) images when the target motion is confined to a two-dimensional plane. It is shown that the adaptive joint time–frequency algorithm provides an effective method of achieving rotational motion compensation for ISAR imaging. Examples provided demonstrate the effectiveness of the adaptive joint time–frequency algorithm with both simulated and experimental ISAR data. Results show that if a target is moving smoothly, standard motion compensation generates a clear image of the target by using the conventional Fourier transform methods. However, when a target performs complex motion such as perturbed random motions, standard motion compensation is not sufficient to generate an acceptable image. In this case, the adaptive joint time–frequency algorithm provides an efficient candidate to resolve the image smearing caused by the time-varying behaviour and leads to a well focused ISAR image when the target motion is confined to a two-dimensional plane. The study also adds insight into the distortion mechanisms that affect the ISAR images of a target in motion.

1 Introduction

Inverse synthetic aperture radar (ISAR) imaging has been around for many years and is used in microwave radar applications such as signature diagnostic and target identification applications. ISAR images of aircraft can provide functional target signatures for non-cooperative target recognition (NCTR) [1, 2]. The problem of NCTR has always been a topic of interest in military operations, for example, in improving situational awareness. Therefore, the ability to generate focused images from ISAR systems is of paramount importance to military and intelligence operations. Since the image is a two-dimensional projection of the target, spatial features present in the ISAR images have the potential of offering sufficient information about the targets for identification purposes [1, 2].

One of the main challenges in ISAR image formation is the unknown nature of the target motion. The essential requirement for ISAR imaging is target rotation. This type of motion produces the Doppler shift required to map the target's reflectivity in the cross-range direction. However, to form an image using the conventional two-dimensional discrete Fourier transform approach, target rotation must be small to avoid blurring of image features. Blurring or image defocusing is caused by a combination of a varying cross-range and range walk. Time-varying Doppler shifts associated with the individual target scattering points must be smaller than the Doppler resolution to prevent distortion in cross-range. Similarly, the range shift incurred by the scatterers must be smaller than the down-range resolution to prevent distortion in the down-range dimension. Blurring is observed whenever the Doppler shift of each scatterer deviates from a constant or if there is a rate of down-range change caused by acceleration, deceleration or turning [3].

Ideally, if the target has only uniform rotational motion and data is collected over a small angular aperture, then a simple Fourier transform process would bring a set of range profiles collected over a given dwell time (i.e. the coherent processing interval) into a focused two-dimensional image. However, actual targets observed by an operational radar rarely have such an ideal motion. Targets are often engaged in complicated manoeuvres that combine translational and rotational motions. For long imaging times i.e. long coherent integration time or for fast manoeuvring targets, simple Fourier processing without compensation will lead to severe image blurring in cross-range. Therefore, motion compensation is needed to generate focused ISAR imagery.

When an aircraft is in motion, small random perturbing rotational motions in pitch, roll and yaw are often produced. Unfortunately, these perturbed motions introduce distortion (e.g. blurring) in the ISAR images [4, 5]. The observation of very large distortions from experimental ISAR data has been reported [6]. These observations clearly show that whenever an aircraft has a complex motion, such as pitching, yawing and rolling, the resulting ISAR image becomes severely distorted. It is very difficult to conduct a definitive study on the distortion phenomenon using in-flight aircraft. For example, there is no information on the location of the target rotational axis and no prior knowledge of the true (static) image of the target for comparison with the analysis. Therefore, we conducted a set

IEE Proceedings online no. 20030670

doi: 10.1049/ip-rsn:20030670

Paper received 13th January and in revised form 23rd May 2003

T. Thayaparan, S.K. Wong and E. Riseborough are with the Surface Radar Section, Defence Research Establishment Ottawa, 3701 Carling Avenue, Ottawa, Ontario, Canada K1A 0Z4

G. Lampropoulos is with A.U.G. Signals Ltd, 1 St. Clair Avenue West, 11th floor, Toronto, Ontario, Canada M4V 1K7

of controlled experiments on the distortion of ISAR images in order to perform a systematic analysis of ISAR images [5]. A numerical model was developed to simulate the distorted ISAR images due to various time-dependent rotational motions that can occur in real in-flight targets [5]. This will allow us to gain new insights and a better understanding of the distortion phenomenon. In this paper, we use an adaptive joint time–frequency algorithm for refocusing distorted ISAR images. This adaptive joint time–frequency algorithm is independently developed by the authors based on the concept introduced by [7, 8]. The objective of this paper is to demonstrate the effectiveness of the adaptive joint time–frequency algorithm for motion compensation using both the simulated and experimental data sets. This study also adds insight into the distortion mechanisms that affect the ISAR images of a target in motion.

2 ISAR motion compensation algorithm

There are many different motion compensation algorithms that deal with target motion effects [1, 2, 8–14]. Since target motion can always be decomposed into translational and rotational motion, a typical motion compensation algorithm consists of a two-step process. First, a point on the target is focused through translational motion compensation. Note that when there is nonuniform rotational motion, other points on the target are not necessarily focused. Rotational motion compensation is then applied to focus these other points. If the rotational motion of the target is confined to a two-dimensional plane, rotational motion compensation of a second point on the target will focus the whole target.

When the coherent processing interval is long or when the target performs rapid manoeuvres, the phase error due to the nonuniform rotational motion is often significant and must also be properly compensated. It has been shown that time–frequency analysis is an attractive way to address the Doppler tracking issue in motion compensation [15–18]. Specifically, it was shown that by applying the time–frequency distribution series in place of Fourier processing, the ISAR image can be effectively examined at each dwell time instant, thus eliminating range drift and Doppler smearing [15–19]. The Doppler resolution achievable in this manner is still less than that offered by the total dwell time of the original data.

Recently, an adaptive joint time–frequency algorithm was introduced by [7, 8] for phase estimation of prominent point scatterers based on the concept of signal parameterisation [20, 21]. In this method, the target motion is modelled as a polynomial function, and an exhaustive search procedure is used to find the motion parameters that are embedded in the phase of the prominent point scatterers. Once the motion parameters are known, compensation of both translational and rotational effects can be achieved. In the following Section, we describe the adaptive joint time–frequency algorithm for achieving both translational and rotational motion compensation. This algorithm is independently developed by the authors based on the concept described in [7, 8].

2.1 Adaptive search procedure and implementation

To form a focused image from raw radar data, it is customary to first carry out a coarse alignment of the data in the range dimension (Fig. 1), followed by fine motion compensation in the cross-range dimension. Joint time–frequency techniques have been shown to be useful tools for carrying out the fine

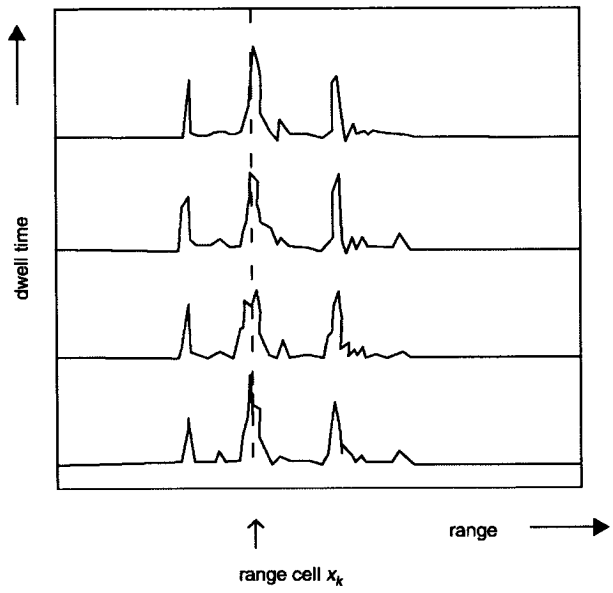

Fig. 1 *Range profiles against dwell time (or pulse number) after coarse range alignment*

motion compensation. A basic assumption is that the target is a rigid body during the data acquisition time. When the target undergoes rigid-body motion, the resulting radar image preserves the spatial features of the target. The target is assumed to exhibit both translational and rotational motion. We assume that the standard range alignment has been applied to the data so that the coarse translational motion has been removed. That is, all the scatterers are located in their respective range cells. We assume that the rotational motion of the target is confined to a two-dimensional plane, i.e. with the fixed rotational axis, during the coherent processing interval. This type of target rotation is termed two-dimensional motion. When the target has a varying rotational axis (i.e. when the rotational motion is not confined to a two-dimensional plane), during the coherent processing interval, the target motion is termed three-dimensional motion [4, 22–24]. Since our measured data from controlled experiments is confined to a two-dimensional plane, we concentrate on the two-dimensional motion. However, we intend to address three-dimensional motion in a future publication.

When the target motion is confined to a two-dimensional plane during the imaging interval, the radar backscattered signal as a function of dwell time t (time index of each pulse) in a particular range cell x can be written as [7, 17]

$$s(x,t)=\sum_{k=1}^{N_k} A_k \exp\left\{-j\frac{4\pi f_0}{c}[R(t)+x_k\cos(\varphi(t))+y_k\sin(\varphi(t))]\right\} \quad (1)$$

where N_k is the number of point scatterers within range cell, f_0 is the centre frequency of the radar and A_k is the the scattering magnitude. (x_k, y_k) denotes the kth point scatterer position, where x_k represents the down-range and y_k represents the cross-range. $R(t)$ describes the residual uncompensated translational displacement and $\varphi(t)$ is the rotational displacement. After coarse range alignment, the residual uncompensated displacement is smaller than the range resolution, but it can still be larger than the radar wavelength. Therefore, either $R(t)$ or $\varphi(t)$ is no longer the simple constant or linear relationship which is assumed for ideal no-motion error ISAR imaging. They can be expanded into polynomial functions of the dwell time via Taylor series as

$$R(t) = R_0 + vt + \frac{1}{2}v't^2 + \frac{1}{3!}v''t^3 \ldots \quad (2)$$

$$\varphi(t) = \Omega t + \frac{1}{2}\Omega' t^2 + \frac{1}{3!}\Omega'' t^3 \ldots \quad (3)$$

By substituting these expressions into (1) and taking the first three terms, we obtain

$$s(x,t) = \sum_{k=1}^{N_k} A_k \exp\left\{-j\frac{4\pi f_0}{c}[a_0 + a_1 t + a_2 t^2 + \ldots]\right\} \quad (4)$$

where

$$a_0 = R_0 + x_k,$$

$$a_1 = v + y_k\Omega \text{ and}$$

$$a_2 = \frac{1}{2}(v' - x_k\Omega^2 + y_k\Omega') \quad (5)$$

The constant phase term a_0 defines the co-ordinate positions of the scatterer on the target. The first-order phase term a_1 contains the radar line-of-sight translational motion and the constant rotational motion of the target. Note that the first-order phase term is a pure linear function of time. In this case, a simple Fourier transform will focus the point scatterers to their respective y_k positions in the cross-range dimension. The second-order and higher-order terms are the source of the phase error that cause image blurring. That is, any coefficients beyond the first-order are detrimental to ISAR image formation. It should be emphasised here that we assume $(\Omega t)^2 \ll 1$ so that this term can be neglected. This is generally a good approximation for CM (centimetre) and MM (millimetre) wave radars, as the angle window needed to form an image with sufficient cross-range resolution is comparatively small in absolute terms (i.e. a few degrees) [17]. With this approximation, the second-order coefficient becomes $a_2 = 1/2(v' + y_k\Omega')$. The first term in a_2 represents the translational motion error and is independent of the cross-range y. The second term in a_2 represents the rotational motion error and is dependent on the cross-range y.

The simplified phase term in (4) can be considered as a sum of polynomials in the time series where the coefficients of each polynomial are determined by the co-ordinates of the scatterers and the target motion parameters. To solve the ISAR motion compensation problem, we need to determine these motion parameters and remove the unwanted nonlinear phase terms from the radar data. Therefore, the goal of the motion compensation algorithm is to estimate and eliminate the second-order phase terms.

If the phase terms in the uncompensated radar signal are time-varying, the instantaneous frequency f_i of each of this components can be expressed as

$$f_i = \frac{1}{2\pi}\frac{d\Phi(t)}{dt} \quad (6)$$

where $\Phi(t) = a_0 + a_1 t + a_2 t^2$.

Therefore, the quadratic phase term in the uncompensated radar signal behaves like a linear chirp in the time–frequency plane. As shown in Fig. 2*a*, the dwell time and Doppler frequency trajectories of the point scatterers within a given range cell are straight lines. The displacement and slope of each line are related, respectively, to the linear and quadratic coefficients of their phase function. The task at hand is to determine these coefficients for the dominant point scatterer within a range cell. This task can be accomplished using the adaptive joint time–frequency procedure. The essential idea of this procedure is to find the basis function that most resembles the strongest signal component in (1). For this problem, a basis function of the form

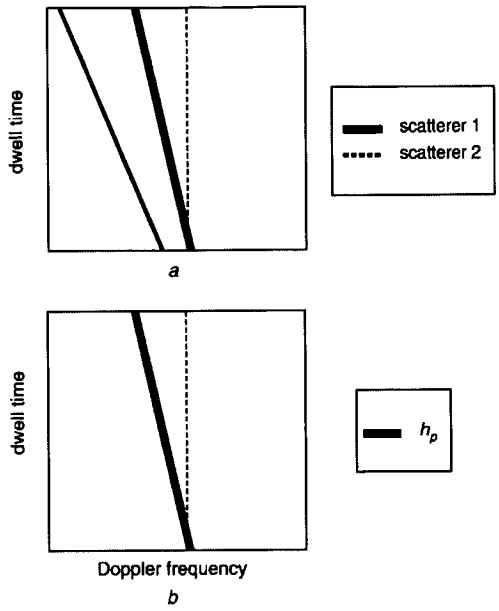

Fig. 2 *Time–frequency representation of the signal in range cell k*

a Time–frequency display of the residual uncompensated radar signal of two prominent point scatterers

b Search procedure for the best basis $h_p(t)$

$$h_p(t) = \exp\left[-j\frac{4\pi f_0}{c}\left(f_1 t + \frac{1}{2}f_2 t^2 + \frac{1}{3}f_3 t^3 + \ldots\right)\right] \quad (7)$$

is used. The above set of basis functions can be thought of as a collection of unit chirps, each with a different displacement and chirp slope [shown as a thick solid line in Fig. 2*b*]. The best function is found by searching for parameters $f_1, f_2, f_3, \ldots$ that maximise the projection from the radar signal onto the basis function. That is

$$\{f_1, f_2, f_3, \ldots\} = \arg\ \max |\langle s(x,t), h_p(t)\rangle| \quad (8)$$

where the projection is formulated as the inner product of the two functions as

$$|\langle s(x,t), h_p(t)\rangle| = \int s(x,t)h_p^*(t)dt \quad (9)$$

Because of the rigid-body assumption, the motion parameters in (5) are carried by every point scatterer on the target. Equation (8) indicates that phase function parameters are estimated in a way that gives maximum projection from the radar data onto the basis function for that prominent point scatterer. We choose to use only the dominant scatterer in a range cell in order to avoid estimation errors for the weaker scatterers. In the search procedure, the linear coefficient f_1 can efficiently be obtained by using the fast Fourier transform, while all other higher terms $f_2, f_3, \ldots$ are obtained by using exhaustive search techniques. In terms of performance, the algorithm is equivalent to picking out the strongest line in the time–frequency plane with the full Doppler resolution offered by the total coherent processing interval.

We illustrate the concept of the adaptive joint time–frequency procedure for residual translational and rotational motion compensation in Figs. 1, 2 and 3. The coarse range alignment is shown in Fig. 1, where all the scatterers are

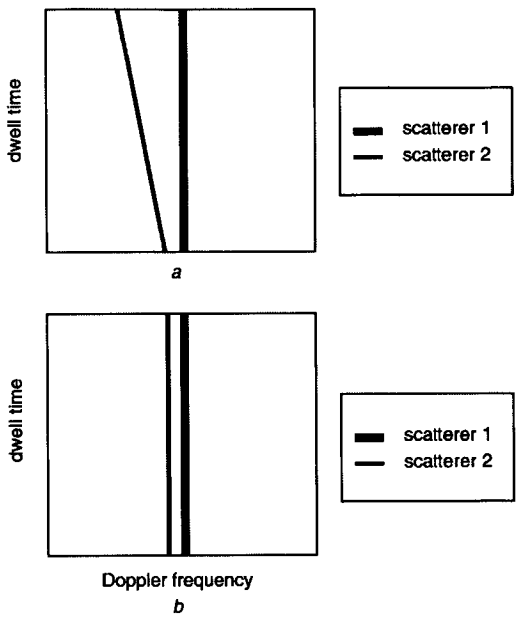

Fig. 3 *Residual translation and rotational motion compensation by adaptive joint time–frequency*

a After translation motion compensation using one promiment point scatterer

b After rotational motion compensation using a second prominent point scatterer

located in the respective range cells. Range cell x_k contains a prominent point scatterer and Fig. 2*a* shows the time–frequency representation of the radar signal at this range cell. Each line in the time–frequency plane represents the time-varying Doppler characteristics of a scatter centre in the range cell. Each chirp represents an individual scatterer. If we assume there are only quadratic phase errors in the data, then the Doppler frequency shifts due to dwell time can be illustrated by linear chirps with different displacements and slopes. The displacement of the line represents the coefficient of the linear phase term and its slope represents the coefficient of the quadratic term. For higher-order phase errors, the radar signal of the scatterer in the time–frequency plane will not be a linear chirp but would be tilted and curved.

The goal of the adaptive joint time–frequency procedure is to find several strong chirp signals and extract their displacement and slope parameters. Fig. 2*b* illustrates the best basis function h_p that resembles a strongest chirp signal in Fig. 2*a* (scatterer 1). The best basis function is found by searching for parameters $f_1, f_2, f_3, \ldots$ that maximize the projection from the radar signal onto the basis function. Once the parameters $\{f_{11}, f_{12}, f_{13}, \ldots\}$ of the first prominent point scatterer are found, the residual uncompensated translational displacement can be removed by multiplying the radar data with the conjugate of the 'found' basis function. The time–frequency display obtained at this stage is illustrated in Fig. 3*a*. It should be noted that the strongest line has been straightened and shifted to the centre of the Doppler frequency (cross-range) axis. Since all the point scatterers share the same residual translation motion in (1), this operation will remove the residual translational motion of the whole target.

After the residual translation motion compensation, the backscattered signal in (1) becomes

$$s(t) = \sum_{k=1}^{N_k} A_k \exp\left\{-j\frac{4\pi f_0}{c}[\Delta x_k + \Delta y_k \varphi(t)]\right\} \qquad (10)$$

where $(\Delta x_k, \Delta y_k)$ is the differential position of the kth scatterer relative to the prominent point scatterer (i.e. (0, 0)) chosen for residual translational motion compensation in the previous step. For rotational motion compensation, a second prominent point scatterer, generally in a range cell different from the first one, is chosen for phase analysis. The same search procedure as described before is repeated for the rotational motion parameters $\{f_{21}, f_{22}, f_{23}, \ldots\}$ in (10). Then to remove the rotational motion, we define a new dwell time variable t' as

$$t' = \frac{1}{f_{21}}(f_{22}t^2 + f_{23}t^3 + \ldots) \qquad (11)$$

The radar data is now uniformly resampled in terms of this new time variable so that the phase of all point scatterers on the target depends linearly on time. Equation (10) now becomes

$$s(x, t') = \sum_{k=1}^{N_k} A_k \exp\left\{-j\frac{4\pi f_0}{c}[\Delta x_k + \Delta y_k \varphi(t')]\right\} \qquad (12)$$

If the phase is linearly dependent on time, then the residual motion due to nonuniform rotation rate is removed from the data. As we can see in the time–frequency display of Fig. 3*b*, both lines are straightened, implying that all the quadratic phase errors are eliminated and that all the points are well focused.

3 Results

We demonstrate the application and effectiveness of the adaptive joint time–frequency motion compensation procedure with simulated radar data and with measured experimental radar data. For simplicity, we consider either a stationary target or perfect translational motion compensation such that the radial velocity of the target is set to zero. In other words, we focus only on the rotational aspect of the target in forming the ISAR image.

3.1 Simulated data

To gain a better physical insight into the scattering phenomenon of an aircraft's ISAR image, an aircraft can be assumed to be composed of a set of point scatterers on a two-dimensional plane. Each scattering point on the aircraft does not represent any geometric point on the target but a combination of scattering sources that return a radar echo. A two-dimensional model of an aircraft's scattering centres is sufficiently adequate to analyse the ISAR images of aircraft. In this simulation we assume the target contains six microwave corner reflectors (i.e. scatterers) to simulate the distorting effect that could occur in ISAR images.

We first test the adaptive joint time–frequency motion compensation algorithm on simulated radar data. Simulated radar data from six corner reflectors is used to demonstrate the adaptive joint time–frequency motion compensation procedure. A picture of the target is shown in Fig. 4. The centre frequency of the radar is 9 GHz and the bandwidth is 300 MHz. A total of 30 range cells and 50 cross-range cells are used for the imaging. In Fig. 5, we show the image from the simulated data without any added motion error as a reference for comparison. This Figure illustrates the undistorted ISAR image when the target is uniformly rotating at a constant rate of 3 degrees/second. Since there are no random motions, we can use the conventional Fourier transform; that is, we take a series of one-dimensional Fourier transforms across the target. As expected, the image is well focused.

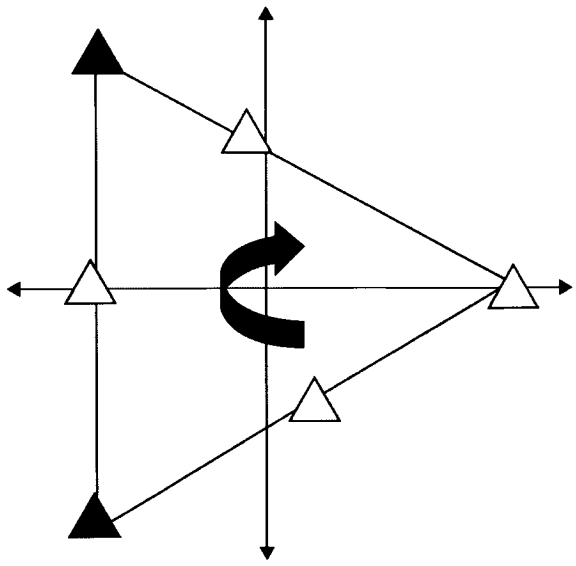

Fig. 4 *Picture of the target contains six simulated corner reflectors*

Then we inject perturbed random motion (or motion error) into the simulation. That is, in addition to the uniform (3 degrees/second) rotation we inject perturbed random motion through a 'sine-drive' by adding an additional sine wave to the motion. The resultant rotational motion will then be a nonuniform. It should be noted here that the rotational motion of the target is confined to a two-dimensional plane during the coherent processing interval. Fig. 6*a* illustrates the distorted image obtained by using the conventional Fourier transform. In this case, the perturbed oscillation is 1 Hz. The Figure clearly shows that the image is severely distorted, which means that the target itself contains much rotational error. The image is smeared along the cross-range direction. This is because of the target's complex motion due to perturbed random motion during the entire coherent processing interval. The conventional radar imaging that uses the Fourier transform, which works well for uniform rotational motion, cannot be directly applied to the perturbed target.

The adaptive joint time–frequency motion compensation algorithm is then applied to this data. Fig. 6*b* illustrates the final image after the rotational motion compensation. All the scatterers are well focused in their individual range and cross-range cells. This implies that all the quadratic phase terms are eliminated.

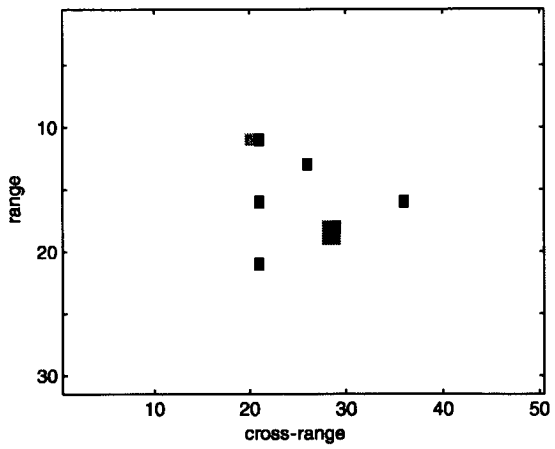

Fig. 5 *Reference ISAR image of simulated corner reflectors data without any motion error*

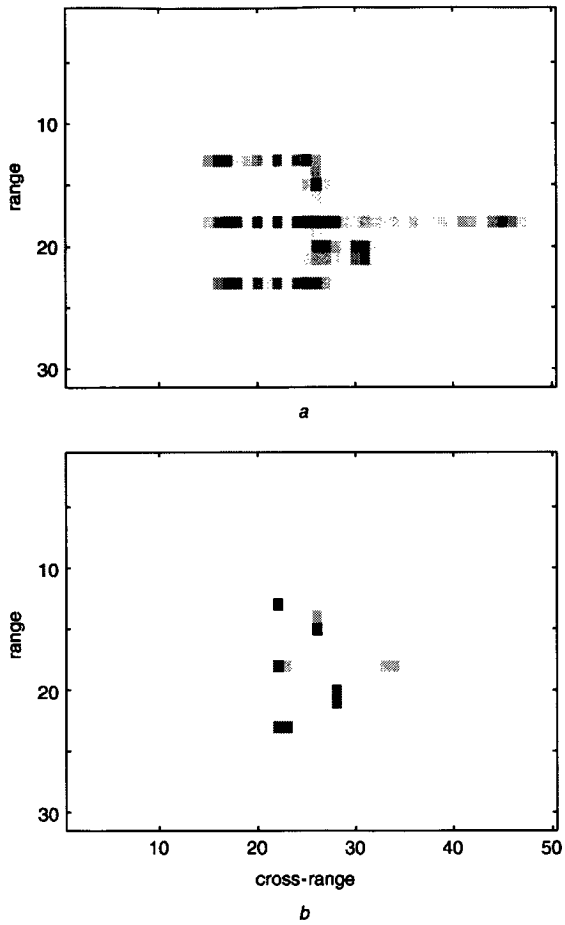

Fig. 6 *ISAR image formation from simulated corner reflectors data*

a ISAR image of simulated corner reflectors using conventional Fourier transform

b Resulting final image after rotational motion compensation

Figure 7*a* illustrates another example of a distorted image due to perturbed random motion error. The image is poorly focused and the image of each scatterer is severely smeared. In this case, the perturbed oscillation is 0.57 Hz. Figure 7*b* shows that the adaptive joint time–frequency motion compensation algorithm successfully eliminates the quadratic phase terms and shows a well focused ISAR image. In Fig. 5, the image from the simulated data without any added motion errors is shown as a reference for comparison. We can see that the motion-compensated image achieves the same sharpness as the reference image.

3.2 Experimental data

We conducted an experimental study to investigate the distortion of ISAR images of moving targets, to develop a numerical model simulation to characterise the distortion behaviour and to examine the time–frequency techniques for restoring distorted ISAR images and to verify our simulated results.

A 5 m by 5 m delta-wing apparatus was constructed to simulate a full size target. A picture of the target is shown in Fig. 8. Six corner reflectors were mounted on the apparatus to simulate the major scattering centres of the target. These six corner reflectors were set to oscillate on their own at a controlled rate to simulate the fluttering effect from aircraft parts or mounted stores on aircraft. The apparatus was mounted on a rotating/heaving table that can produce rotational motions at a controlled rate. These rotational motions were confined to a two-dimensional plane.

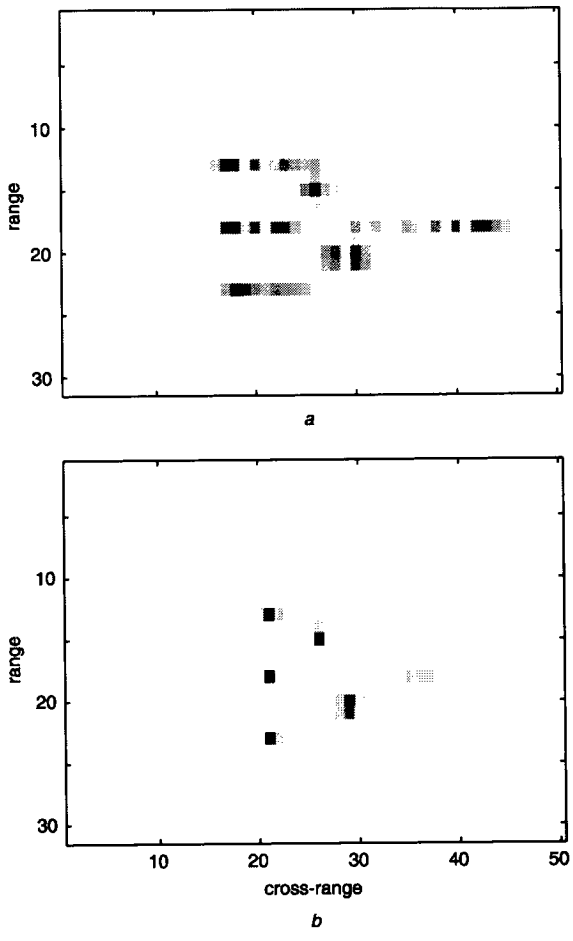

Fig. 7 *ISAR image formation from simulated corner reflectors data*

a ISAR image of simulated corner reflectors using conventional Fourier transform

b Resulting final image after rotational motion compensation

Therefore, data from this pseudo point-source target permits an easier and a more definitive analysis of the residual motion effects on ISAR images.

The radar data was collected using a ground radar having a centre frequency of 9.05 GHz and a bandwidth of 300 MHz. A total of 50 range cells and 50 cross-range cells are used for the imaging. To demonstrate the effectiveness of the adaptive joint time–frequency motion compensation algorithm, we tested our algorithm on two measured radar data sets. We apply both the Fourier-based and time–frequency-based image formation to a set of measured radar data.

The first measured data set contains nonuniform rotational motion in which the perturbed random motion is less than 1 Hz. Figure 9*a* shows the resulting ISAR image from taking a series of one-dimensional Fourier transforms across the dwell time. Since significant phase errors due to nonuniform rotational motion exist in the data, the image is quite blurred in the Doppler dimension. It is not possible to distinguish individual scatterers because some of the scatterers are severely blurred. We then applied the adaptive joint time–frequency motion compensation algorithm on the data. Figure 9*b* illustrates the final image after the rotational motion compensation. All the corner reflectors are focused in the image. That is, the image is focused in range and cross-range.

The second measured data set contains nonuniform rotational motion in which the perturbed random motion is more than 1 Hz. Figure 10*a* illustrates the resulting image after taking a series of one-dimensional Fourier transforms across the dwell time. This image is very severely distorted and scatterers are indistinguishable from one another. The image is severely blurry in the Doppler dimension. The fuzzy image clearly shows that significant amount of rotational motion errors exist in the data. Figure 10*b* shows the final image after the rotational motion compensation. The Doppler smearing is significantly reduced and the image shows dramatic improvement over that shows in Fig. 10*a*. The image is now focused and the six corner reflectors of the target are clearly visible.

Generally the results show that experimental focused images are somewhat less focused than simulated data. Scatterers are considered to be isotropic during long coherent integration time. However, angular dependencies and masking effects may degrade the experimental focusing processing. It should be noted that the scatterer distribution in Figs. 9 and 10 does not match the position of trihedrals shown in Fig. 8 as one scatterer is displaced. The reason is that one corner reflector was offset from the centre to aid in the analysis of the target by enabling us to discern the orientation of the platform from the resultant ISAR images.

Fig. 8 *Picture of the target motion simulator experimental apparatus*

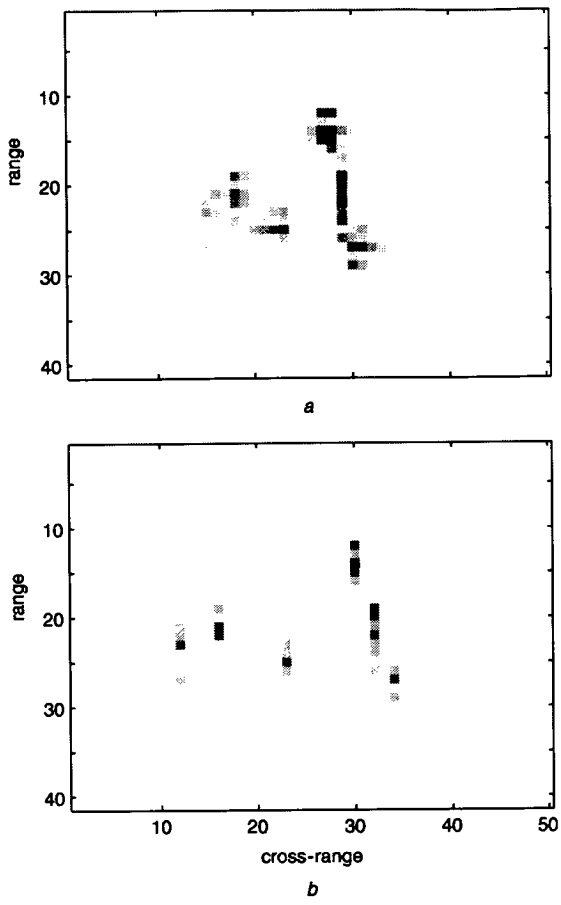

Fig. 9 *ISAR image formation from experimental radar data*

a ISAR image of measured corner reflectors using conventional Fourier transform

b Resulting final image after rotational motion compensation

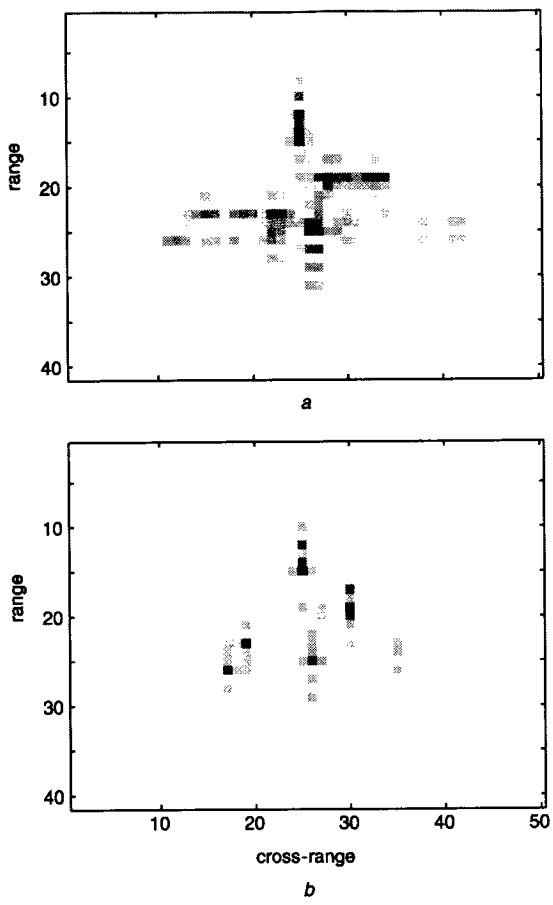

Fig. 10 *ISAR image formation from experimental radar data*

a ISAR image of measured corner reflectors using conventional Fourier transform

b Resulting final image after residual rotational motion compensation

The image quality was checked using PSLR (peak sidelobe ratio) and ISLR (integrated sidelobe ratio). It has been found on average that the improvements in PSLR are in the range 2–20 dB while the improvements in ISLR are in the range 1–5 dB. We see that the adaptive joint time–frequency motion compensation algorithm performed well in achieving a focused image of the target. It should be noted that these results are preliminary and more data has to be analysed to evaluate the consistency of the adaptive joint time–frequency motion compensation algorithm. We intend to do this in the near future.

One drawback of the adaptive joint time–frequency method is the computational burden associated with the exhaustive search procedure for the motion parameters. This problem becomes especially severe when higher-order motion effects are involved. Recently, generic algorithms have been attempted as a way to reduce the computational complexity and speed up the search procedure [25, 26].

4 Conclusions

When target motion is confined to a two-dimensional plane during coherent processing intervals, the adaptive joint time–frequency algorithm is shown to be an effective method for achieving rotational motion compensation in ISAR imaging. We have illustrated the algorithm using both simulated and measured experimental radar data sets. The results show that the adaptive joint time–frequency algorithm performed very well in achieving a focused image of the target. Results also demonstrate that adaptive joint time–frequency techniques can significantly improve the distorted ISAR image over what can be achieved by conventional Fourier transform methods when the rotational motion of the target is confined to a two-dimensional plane. This study also adds insight into the distortion mechanisms that affect the ISAR images of a target in motion.

5 References

1 Ausherman, A., Kozma, A., Waker, J.L., Jones, H.M., and Poggio, E.C.: 'Development in radar imaging', *IEEE Trans. Aerosp. Electron. Syst.*, 1984, **20**, pp. 363–400

2 Chen, C.C., and Andrews, H.C.: 'Target motion induced radar imaging', *IEEE Trans. Aerosp. Electron. Syst.*, 1980, **16**, pp. 2–14

3 Son, J.S., Thomas, G., and Flores, B.C.: 'Range-Doppler radar imaging and motion compensation' (Artech House, Boston, MA, USA, 2000)

4 Chen, V.C., and Miceli, W.J.: 'Effect of roll, pitch and yaw motions on ISAR imaging', *Proc. SPIE – Int. Soc. Opt. Eng.*, 1999, **3810**, pp. 149–158

5 Wong, S.K., Duff, G., and Riseborough, E.: 'Analysis of distortion in the high range resolution profile from a perturbed target', *IEE Proc., Radar Sonar Navig.*, 2001, **148**, pp. 353–362

6 Sparr, T., Hamran, S.-E., and Korsbakken, E.: 'Estimation and correction of complex target motion effects in inverse synthetic aperture imaging of aircraft'. IEEE Radar 2000 Conf. Record, Alexandria, VA, USA, May 2000

7 Ling, H., Wang, Y., and Chen, V.C.: 'ISAR image formation and feature extraction using adaptive joint time-frequency processing', *Proc. SPIE – Int. Soc. Opt. Eng.*, 1997, **3708**, pp. 424–432

8 Wang, Y., Ling, H., and Chen, V.C.: 'ISAR motion compensation via adaptive joint time-frequency technique', *IEEE Trans. Aerosp. Electron. Syst.*, 1998, **34**, pp. 670–677

9 Jain, A., and Patel, I.: 'SAR/ISAR imaging of a nonuniformly rotating targets', *IEEE Trans. Aerosp. Electron. Syst.*, 1992, **28**, pp. 317–321

10 Colloway, T.M., and Donohoe, G.W.: 'Subaperture autofocus for synthetic aperture radar', *IEEE Trans. Aerosp. Electron. Syst.*, 1992, **30**, pp. 617–621

11 Itoh, T., Sueda, H., and Watanabe, Y.: 'Motion compensation for ISAR via centroid tracking', *IEEE Trans. Aerosp. Electron. Syst.*, 1996, **32**, pp. 1191–1197

12 Carrara, W.G., Goodman, R.S., and Majewski, R.M.: 'Spotlight synthetic aperture radar - signal processing and algorithms' (Artech House, Boston, MA, USA, 1995)
13 Rihaczek, A.W., and Hershkowitz, S.J.: 'Radar resolution and complex-image analysis' (Artech House, Boston, MA, USA, 1996)
14 Werness, S., Carrara, W., Joyce, L., and Franczak, D.: 'Moving target imaging algorithms for SAR data', *IEEE Trans. Aerosp. Electron. Syst.*, 1990, **26**, pp. 57–67
15 Chen, V.C.: 'Reconstruction of inverse synthetic aperture images using adaptive joint time-frequency wavelet transforms', *Proc. SPIE – Int. Soc. Opt. Eng.*, 1995, **2491**, pp. 373–386
16 Chen, V.C., and Qian, S.: 'Joint time-frequency transform for radar range-Doppler imaging', *IEEE Trans. Aerosp. Electron. Syst.*, 1998, **34**, (2), pp. 486–499
17 Chen, V.C., and Ling, H.: 'Time-frequency transforms for radar imaging and signal analysis' (Artech House, Boston, MA, USA, 2002)
18 Qian, S., and Chen, D.: 'Joint time-frequency analysis: methods and applications' (Prentice-Hall Inc., New York, USA, 1996)
19 Qian, S., and Chen, D.: 'Decomposition of the Wigner-Ville distribution and time-frequency distribution series', *IEEE Trans. Aerosp. Electron. Syst.*, 1994, **42**, pp. 2836–2842
20 Qian, S., and Chen, D.: 'Signal representation using adaptive normalized Gaussian functions', *Signal Process.*, 1994, **36**, pp. 1–11
21 Mallat, S.G., and Zhang, Z.: 'Matching pursuits with time-frequency dictionaries', *IEEE Trans. Signal Process.*, 1993, **41**, pp. 3397–3415
22 Li, J., Ling, H., and Chen, V.C.: 'An algorithm to detect the presence of 3D target motion from ISAR data', *Multidimens. Syst. Signal Process.*, 2003, **14**, pp. 223–240
23 Li, J., and Ling, H.: '3D ISAR image reconstruction of a target with motion data using adaptive feature extraction', *J. Electromagn. Waves Appl.*, 2001, **15**, pp. 1571–1587
24 Li, J., Wang, Y., Bhalla, R., Ling, H., and Chen, V.C.: 'Comparison of high-resolution ISAR imagery from measured data and synthetic signatures', *Proc. SPIE – Int. Soc. Opt. Eng.*, 1999, **3810**, pp. 170–179
25 Goldberg, D.E.: 'Genetic algorithms in search, optimization and machine learning' (Addison–Wesley, Reading, MA, USA, 1989)
26 Li, J., and Ling, H.: 'ISAR motion detection and compensation using genetic algorithms', *Proc. SPIE – Int. Soc. Opt. Eng.*, 2001, **4391**, pp. 380–388